BULLETIN OF THE EARTHQUAKE
RESEARCH INSTITUTE
Vol. 49 (1971), pp. 19-32

3. A *Fault-Origin Model of the Great Kanto Earthquake of 1923 as Deduced from Geodetic Data.**

By Masataka ANDO,
Earthquake Research Institute.

(Read September 21, 1970.—Received January 30, 1971.)

Abstract

The writer determined fault parameters of the great Kanto earthquake of 1923 on the basis of the geodetic data by triangulation and levelling. Thus he attempted to establish a dislocation model which reasonably explains all the available data on the surface displacements associated with this earthquake.

Basically the fault line is assumed to extend from the Kozu area southeastward with its strike N45°W, parallel to the trend of the Sagami trough. The shape of the fault plane is assumed to be a rectangular plane. The fault models which was finally accepted is as follows.

total length: 130 km, width: 65 km, dip. 45° and a fault displacement: 6 m (right lateral strike slip) and 3 m (reverse dip slip). Generally speaking, this earthquake seems to indicate a differential movements of the two crustal plates bounded by the Sagami trough. The fault's dimension, geometry and direction of the slip are all in good harmony with the seismological evidence on wave radiation.

1. Introduction

Recently anomalous vertical deformation in the Boso and Miura peninsulas has drawn the scientists attention again to the great Kanto earthquake of Sept. 1, 1923. Specially so, as the high rates of anomalous uplift revealed by precise levelling executed by the Geographical Survey Institute (G.S.I.) may herald an earthquake of similar magnitude and prediction appears in this case to be possible. Despite intensive scientific and engineering studies by many investigators, little was known about the origin of this particular earthquake, the exact location of the epicenter, and the dimension, geometry and location of the fault associated with this earthquake. Recently Kanamori and Miyamura (1970) interpreting the necessary seismograms from various countries re-located its epicenter more accurately. Kanamori (1969) analysed the geodetic

* Comminucated by K. Kasahara.

data in connection with amplitude to propose source-parameters, such as the dimension and geometry of the proposed fault origin model. However some ambiguities remained, especially on the strike of the fault as anticipated by Kanamori who envisaged the possibility of future modification. Kasahara (1970) and Matsuda (1970) discussed geologic and geodetic data and concluded that the neotectonics in the South-Kanto district, including the earthquake of 1923, is attributed to a large submarine fault of right-lateral reverse sense, running south-eastward along the Sagami trough.

In the present paper, the author applies the static, elastic dislocation theory to the surface deformation associated with the Kanto earthquake in order to determine the fault parameters at its origin. Method was developed by Savage and Hastie (1966) using the Alaskan earthquake of 1964. Similar studies were made by Savage and Hastie (1969) on the Fairview Peak Nevada earthquake of 1954, Plafker and Savage (1970) on the Chilean earthquake of 1960 and Hastie and Savage (1970) on the Alaskan earthquake of 1964.

2. Location of the fault trace

A fault trace is defined as the intersection of the fault plane and the earth's surface. It is assumed that the fault trace of the great Kanto earthquake extends from a point adjacent to Kōzu and strikes N45°W, based on the following evidence:

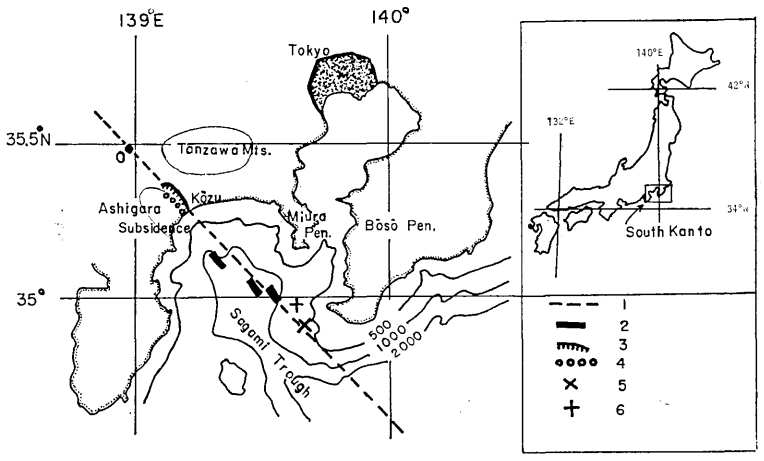

Fig. 1. Sketch map of the south Kanto district (right), assumed fault trace and supporting evidence of it. 1, assumed fault trace; 2, submarine faults after Kimura et al. (1971), 3, Kozu-Matsuda fault; 4, fracture trace of the great Kanto earthquake after Kaneko (1969); 5, location of submarine cables cut; 6, location dead fishes.

(1) the Sagami trough trends N45°W,

(2) a series of steep cliffs exist along the northeastern periphery of the trough (Mogi, 1953), which seems most likely represent fault scraps,

(3) submarine faults parallel to the trough were discovered by Kimura, Kagami, Honza and Nasu (1971), which cut the Plio-Pleistocence Sagami group sediments,

(4) on the coast of the Sagami Bay, the Kōzu-Matsuda fault strikes N40°W, and is regarded as the northwestern extension of the Sagami submarine fault along the trough, which on land separates the Tanzawa mountains from Ashigara area of subsidence.

Further several events during the great Kanto earthquake support this assumption;

(1) submarine cables broke in the Sagami Bay, at the location of 139°40′E and 34°50′N (Land Survey Department, 1926),

(2) a great number of fish were killed and floated up near the above-mentioned area (Land Survey Department, 1926),

(3) Kaneko (1969) attributed several fracture traces near Kōzu to the great Kanto Earthquake.

3. Dip direction of the fault plane and direction of the slip vector in it.

The dip direction of the fault plane and the direction of the strike-slip component of the faulting are derived from the horizontal movements of the crust, which are illustrated as arrows in Fig. 2. These reduced data were compiled by Muto (1932) who revised the original data by the Land Survey Department (1928). The triangulation net in the southern Kanto district was first surveyed in 1894 and resurveyed immediately after the earthquake in 1925. It is evident from Fig. 2 that the faulting has right-lateral strike slip component and that the amplitudes of displacement vectors on the northeastern side of the assumed fault

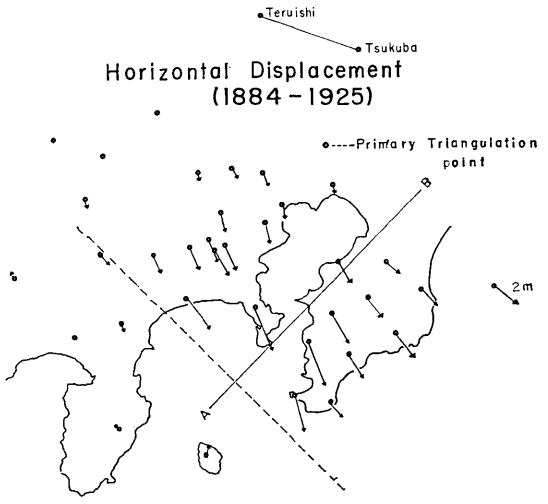

Fig. 2. Horizontal displacement, from Muto (1932).

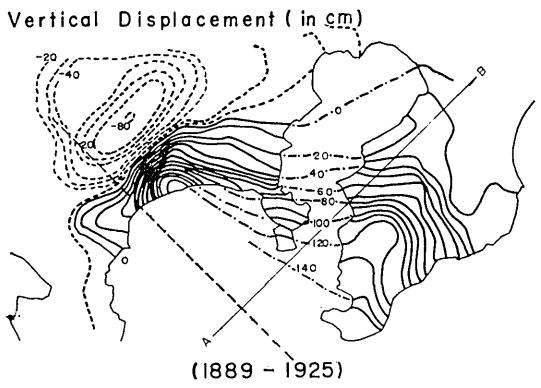

Fig. 3. Vertical displacement, after Miyabe (1934), solid and dashed contours represent elevation and subsidence respectively. Chain lines drawn by the author.

trace (broken line) are greater than those on the other side. This suggests that the fault plane dips northeastward, i.e., the northeastern block is a hanging wall and the southwestern block, a foot wall. Kasahara (1959) and Walsh (1969) suggested that the surface displacements on the side of the hanging wall is generally greater than those on the side of the foot wall.

Fig. 3 shows the vertical movements of the earth's surface revealed by levelling (1894–1924). This figure (Miyabe, 1934) was obtained by high cut filter processing of the results of the Land Survey Department (1926). It is clear from the figure that in the northeastern block the amplitude of uplift decreases with the distance from the fault. Since the fault plane dips northeastward, this trend suggests that faulting had a reverse components. It is thus assumed that the fault plane dips northeastward and has a right-lateral slip and a reverse dip-slip component.

4. Methods of analysis

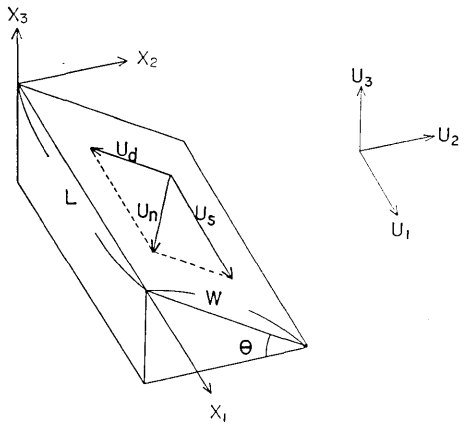

Fig. 4. Relation of dislocation model and surface displacements to the cordinate system. U_1, U_2 and U_3 denote surface displacement vector parallel to X_1, X_2 and X_3 respectively.

Based on a simple dislocation model, the fault parameters of this earthquake are obtained, by changing its parameters, in a trial and error manner until we arrive at the best fit. Maruyama (1964) has given theoretical expressions for the surface deformation associated with a Volter dislocation, which may be used arbitrarily for the dislocation surface and direction of the slip vector. In a simple model the dislocation surface is represented by a rectangular plane with horizontal length L and width W, dipping at angle θ. The

dislocation plane is considered to reach the free surface, i.e., the depth to the upper edge of the plane is equal to zero. Slip on the dislocation surface has two components as mentioned before: U_d and U_s denoting the reverse dip-slip and the right-lateral strike-slip components respectively. Thus the dislocation model is defined by the independent parameters L, W, θ, U_d and U_s, where the slip is assumed to be uniformed all over the dislocation surface. When this model is applied, it is necessary to tie one corner of the dislocation surface on the assumed fault trace. The coordinate system which will be used is shown in Fig. 4.

5. General pattern of the surface deformations

Before discussing the fault parameters quantitatively, it is necessary to examine the basic patterns of horizontal and vertical displacements on the free surface due to a dislocation of a general type, i.e., the one having both strike-slip U_s and dip-slip component U_d. The writer tested several sets of the U_d and U_s values, as examples. The surface displacement field was calculated for the parameters of $L/W=$ 1/1, 2/1, 4/3, 4/1 and $\theta=15°$, 30, 45°, 60°. (Fig. 5a to 5d shows the results thus obtained, for the case of $L/W=2/1$, $\theta=45°$ and $U_n=1$, where $U_n=\sqrt{U_d^2+U_s^2}$.) It should be noted the pattern of the displacement field is not seriously affected by changing the parameters over this range. The general sense of the deformation may be summarized as follows; (1) U_d gives negligible contribution to the horizontal displacement parallel to the strike of the fault, (2) when U_d is zero, vertical displacement still occurs at the end of the fault trace (see Fig. 5b). In the central part, however, horizontal displacement is dominant as indicated by the arrows parallel to the fault line. (3) In the present case surface deformation can be represented by superposition of both of U_d and U_s. It is clear that the deformation thus synthesized is very similar to the observed pattern, with respect to their basic mode. This proves that a Voltera dislocation in elastic half space can explain the observed crustal deformation reasonably.

6. Parameters

Discussion in the previous section has led us to a conclusion that anomalous uplift or subsidence tends to appear around extremities of the fault trace, causing concentration of the equai-value lines of vertical movements. This effect suggests that we can approximately locate the extremities of a fault trace by searching where equi-value lines are concentrated as discussed above. In fact, the remarkable subsidence in the Tanzawa mountains and its vicinity can be attributed to this

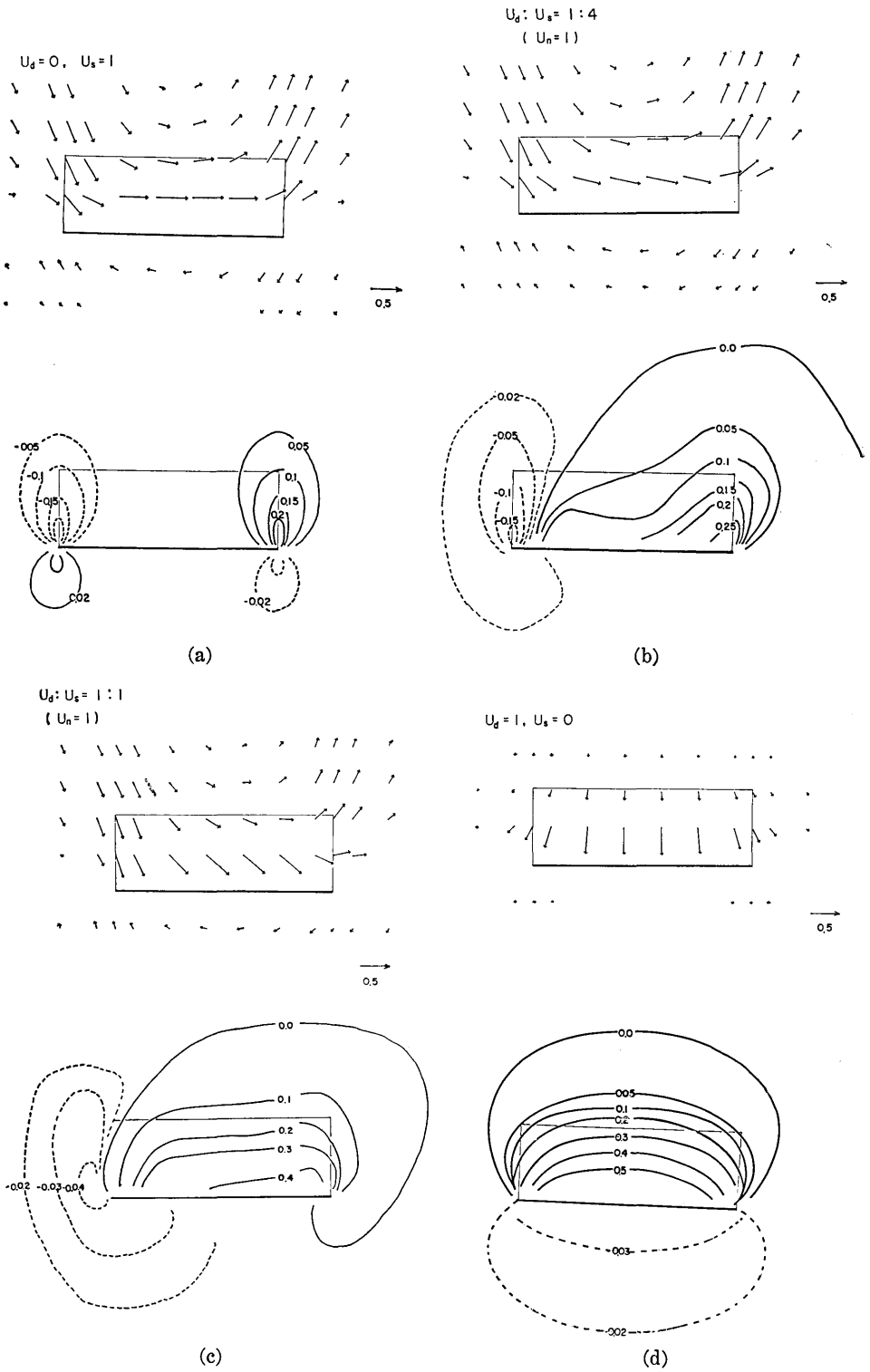

Fig. 5. Calculated surface horizontal and vertical displacements.

effect. One of the fault's extremities can therefore be fixed at point O (Fig. 1), which happens to coincide with the origin of the coordinate system.

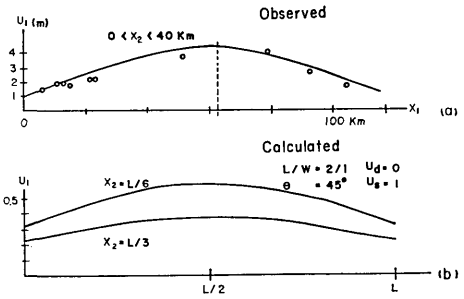

Fig. 6. Distribution of U_1 along the fault line, (a) observation (b) calculation.

The next step is to estimate the length of the fault. Fig. 6 illustrates a result of numerical calculation based on the Maruyama's expression for U_1 due to U_s, where U_1 denoting the horizontal displacement parallel to the fault trace. U_1 becomes maximum at the fault center and decreases gradually away from it. An example for the case of $\theta=45°$ and $L/W=2/1$ is shown in Fig. 6. A similar trend is also noticed on the geodetic data of horizontal displacement as shown in the same figure. Comparison of the theory with observations leads us to a natural conclusion that the maximum value of U_1 is seen at about 65 km from the point O, and consequently, the fault length, L, is 130 km, approximately. The dip-slip and strike-slip components of the dislocation give the negligible contributions to U_1 and U_2 respectively, so far as central part of the field is concerned. This relation enables us to deduce U_d and U_s separately from the respective data of U_2 and U_1. In Fig. 7, amplitudes of the observed U_1 (strike slip) are plotted against the distance from the fault trace, where the solid lines are drawn manually to smooth the observations. Thus, tne amplitudes of the northeastern and southeastern blocks are estimated at 5 m and 1 m, respectively. Similarly, the levelling on U_3, which is plotted in Fig. 8, reveals that the hanging wall of the fault has been uplifted about 1.5 m. However, U_d can not be obtained immediately from this information because the dip angle is not known yet. Let us assume θ

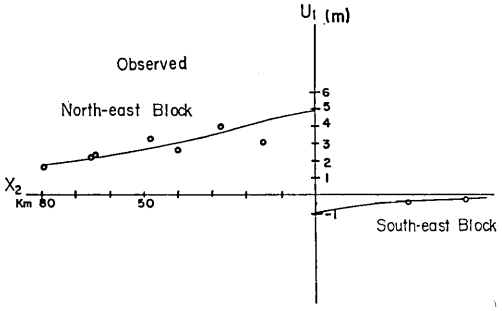

Fig. 7. Diminution curve of observed U_1 along the profile A-B in Fig. 2.

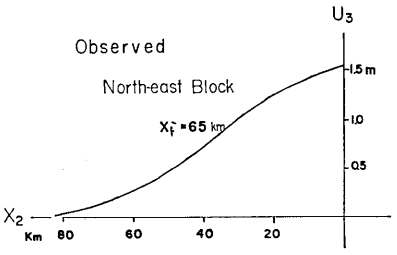

Fig. 8. Diminution curve of elevation in the northeast block along the profile A-B in Fig. 3.

and W to be 15°, 30°, 45° and 60°, and $L/4$, $L/2$, $3L/4$ and L, respectively, we shall thus test the sixteen different sets of L and W to find the most reasonable fit. According to Kanamori and Miyamura (1970) and Kanamori (1971), the focal depth of the main shock is shallower than 10 km, whereas the largest aftershock during the first 24 hour after main shock is located at about 30 km. It may be empirically accepted that spatial distribution of aftershocks during a few days after the main shock reflects configuration of the fault plane. Then, the depth of the present fault plane is safely assumed to be about 30 km, or at least less than 60 km. Under these considerations, reasonable models are chosen from the sixteen sets as shown in Table 1. Amplitudes of calculated U_1 at $X_1=$ 65 km are plotted against the distance from the fault trace in Fig. 9, where broken lines represent smoothed observed value. It is extremely, difficult, of course, to determine θ and L/W precisely, becase only a single profile of the displacement field is available.

Table 1. Depth of the fault plane

(in kilometer)

θ \ W	130 km ($2L$)	100 km ($3L/2$)	65 km (L)	33 km ($L/2$)
30°	113	78	56	28
45°	91	71	46	23
60°	65	50	34	16
75°	34	26	17	9

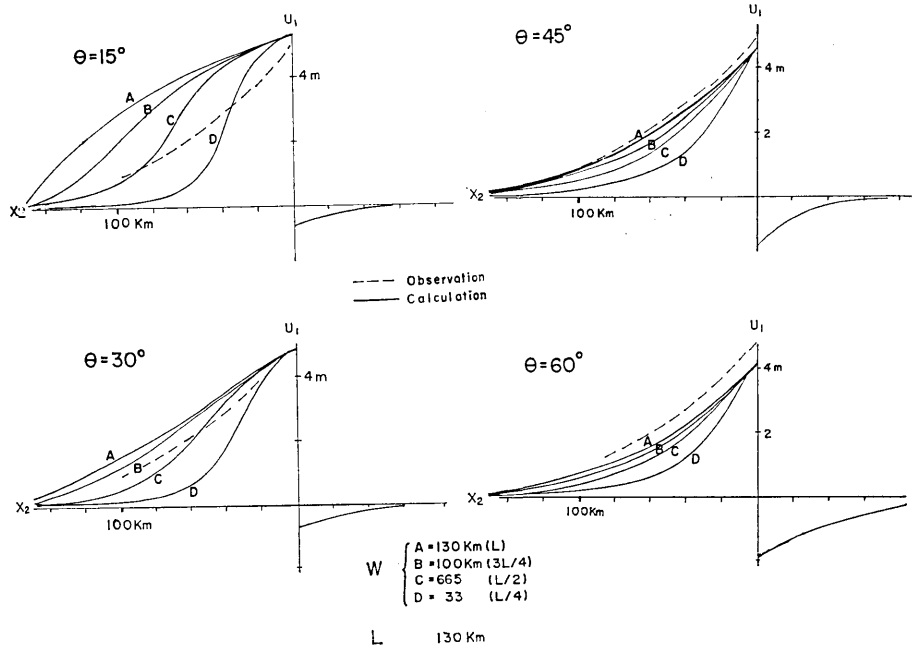

Fig. 9. Diminution curve of calculated U_1 along X_1-65 km for various values of W and θ, broken lines representing the observed value.

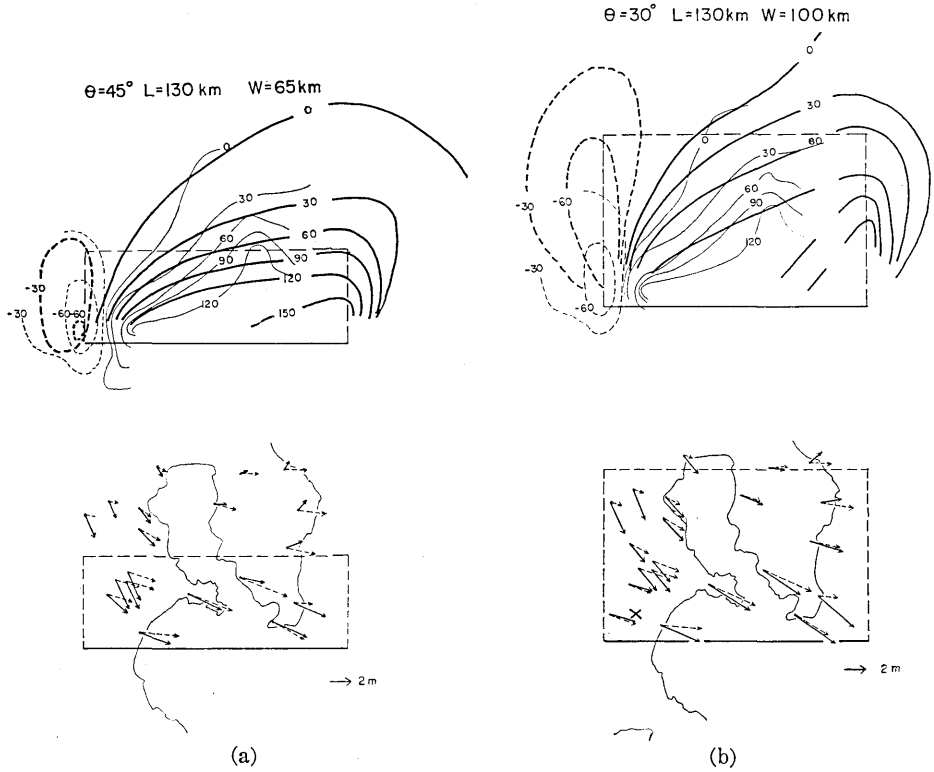

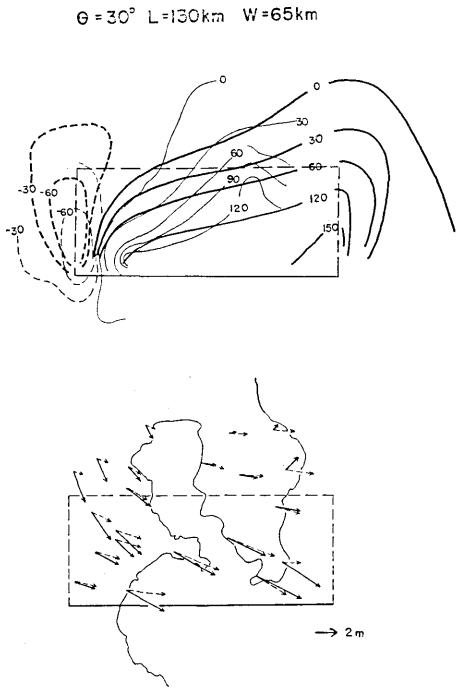

Fig. 10a. b. c. Most likely fault madels
(Upper) Vertical surface displacements (in cm), solid and dashed contours represent elevation and subsidence respectively, thick and fine lines calculation and observation respectively.
(Lower) Solid and dashed arrows represent calculated and observed horizontal displacement respectively.

Therefore, the parameter's values given in the following may fluctuate over a wide range. Thus, the writer tentatively prefers three sets of parameters, i.e., $\theta=45°$—$L/W=2/1$, $\theta=30°$—$L/W=4/3$ and $\theta=30°$—$L/W=2/1$, as the most likely solution. Fig. 10a, b and c show these solution. From these figures, we learn that the preferred dislocation model is Fig. 10a; $L=130$ km, $W=65$ km, $\theta=45°$, $U_s=6$ m, $U_d=3$ m and the location of the one corner of this fault trace is settled at point O (Fig. 1).

7. Discussion

Although these models explain the horizontal displacement pattern equally well, Fig. 10a seems most preferable as it fits better than the other two (Figs. 10b, c). For this reason Fig. 10a is preferred finally. The author believes that this model represents the fault's conditions well, because the location and geometry of the fault as derived geodetically from this model agrees well with those from the seismological model by Kanamori (1971). That is to say, the dip angle of the present model is consistent to the one based on the fault-plane solution by P-wave data (34°), and the amplitude ration of the dip-slip component to the strike-slip one (0.58 unit dip-slip to 0.82 unit strike-slip is also in good agreement with the Kanamori's solution (1971). The fault length of the geodetic model, 130 km, is equal to his solution, too, which is derived from the aftershock area. A slight discrepancy between the geodetic and seismological models is noticed on the fault's width, but this discrepancy might not be very serious in view of various error sources in calculation. The strike of the fault is estimated at about N45°W which coincides very well with the general trend of the Sagami trough as well as with the models by Kasahara (1970) and Matsuda (1970).

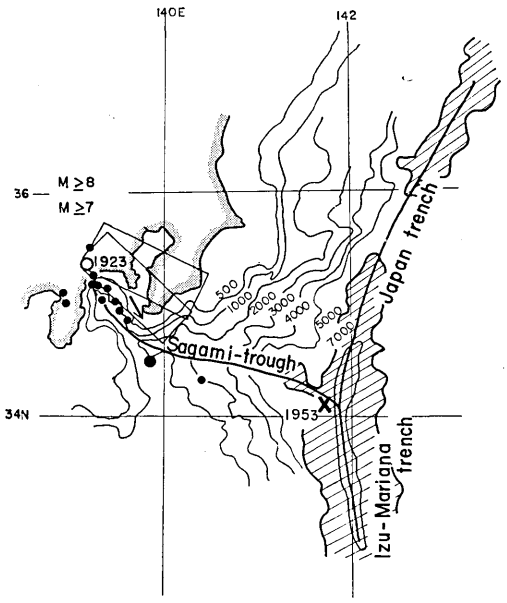

Fig. 11. Rectangular planes with the strike of N45°W and N70°W represent the fault models deduced from geodetic and seismological data respectively. Open circle show the relocated epicenter of the great Kanto earthquake after Kanamori and Miyamura (1970) and solid circles the location of historical great earthquakes after Kawasumi (1951).

However, the strike of corresponding the nodal plane of the *P*-wave solution has been determined to be N70°W (Kanamori, 1971) with which the present data does not agree so well. There are many faults in Miura and Boso peninsulas as discovered by Kaneko (1969), some of them are active and in a trend similar to the solution of Kanamori's i.e., right lateral and thrust with strikes of N60°–70°W. The present writer considers, however, that these are rather miner events in comparison with the above-stated fault. The tectonic setting of the southern Kanto district, discussed by Matsuda (1970) in detail, indicates the strike of the submarine fault about N40°W. This evidence seems to favor the geodetic strike of the fault rather than the seismological one. As discussed previously, geodetic fault model harmonizes with the seismological results in many respects.

The most notable discrepancy between the two models is, perhaps, the net slip in the fault plane. Slip amplitudes, which is derived from the geodetic model is about 6.7 m whereas the seismological, 2 m, approximately. This discrepany seems too large for an error in computation. The writer recalls the similar effects observed in some other cases and considers that these discrepancies reflect on the focal processes. For the Nankaido earthquake of 1946, Alaskan earthquake of 1964 and Niigata earthquake of 1964, the fault's slips are calculated as shown in Table 2. The geodic slip exceeds the seismological slip significantly. Geodetic and seismological refer to differnnt time-bases. One of possible explanations for this discrepancies is therefore attributed to the fact that time constants for the displacements differ in seismic radiation and geodetic deformation. Generally, the seismological slip refers to a fracturing, or wave radiation on relatively short time base, say, several minutes, whereas the geodetic data represent the deformation which accumulated for a longer time. Deformation having a time constant

Table 2. Displacement on the fault plane deduced from geodetic and seismological data

(in meter)

	Magnitude	Geodetic		Seismological	
Kanto (1923)	(8.3)	6.7	(1)	2.1	(2)
Nankaido (1945)	(8.1)	10 (5~18)	(3)	3~5	(4)
Alaska (1964)	(8.5)	15.8	(5)	7	(6)
Niigata (1964)	(7.5)	8	(7)	4	(8)

(1) Present paper
(2) Kanamori: (1971),
(3) Fitch et al. (1971),
(4) Kanamori (personal communication),
(5) Hastie et al. (1970),
(6) Kanamori (1970),
(7) Ando (1971),
(8) Aki (1964)

longer than several minutes can not contribute to the generation of seismic waves.

The agreement of the origin to the fault plane for the geodetic and seismic model is another interesting aspect. The hypocenter of this earthquake from *P*-wave solution located just at the corner of the fault plane which was independently decided from the observed vertical displacement field which also explains the shallowness at the hypocenter.

This earthquake was accompanied with reverse right lateral faulting, and this fault runs along the eastern boundary of the Sagami trough which can be considered as the surface trace of the fault system. The Sagami trough extends from the eastern submarine slope in the Sagami Bay southeastward as far as the junction of the Japan trench with the Izu-Mariana trench in Fig. 11. Along the trough some of historical great earthquakes occured (Kawasumi, 1951). The Boso-oki earthquake of 1953 ($M=8.0$) whose epicenter is located just at the junction should be noted.

In summary, the mechanism of the great Kanto earthquake of 1923 is well explained, both geodetically and seismologically by a differential movement of the two crustal plates which are bounded by a large submarine fault along the Sagami trough.

Acknowledgement

The author would like to thank Prof. K. Kasahara for suggesting this problem, stimulating discussion and critical reading of the manuscript.

He is also thankful to Dr. G. J. Lensan and Prof. H. Kanamori for valuable suggestions.

Dr. Lenson read the manuscript critically. Several helpful advices by Drs. T. Matsuda, K. Nakamura and A. OKada are gratefully acknowledged.

References

AKI, K., Generation and propagation of G waves from the Niigata earthquake of June 16, 1964, *Bull. Earthq. Res. Inst.*, **44** (1964), 73-88.

ANDO, M., Faulting of the Niigata earthquake as deduced from geodetic data (in preparation).

FITCH, T. J. and SCHOLZ, C. H., Mechanism of underthrusting in Southwest Japan: A model of convergent plate interactions, *J. Georphys. Res.*, **76** (1971) (in press).

HASTIE, L. M., A dislocation model for the 1964 Alaska earthquake, *Bull Seism. Soc. Am.*, **60** (1970), 1389-1392.

Land Survey Department, The change of elevation of Land caused by the great earthquake of September 1st. 1923, *Bull. Earthq. Res. Inst.*, **1** (1926), 65-68.

Land Survey Department, Provisory map showing the horizontal displacements of the

primary triangulation points in Kwanto districts, observed after the great earthquake of Sept. 1. 1923, *Bull. Earthq. Res. Inst.*, **4** (1928), 231.

KANAMORI, H., Seismicity and structure of crust and mantle, (translation of the Japanese title), *Kagaku (Science)*, **39** (1969), 474-482, (in Japanese).

KANAMORI, H., The Alaskan earthquake of 1964: radiation of long-period surface waves and source mechanism, *J. Geophys. Res.*, **75** (1970), 5029-5040.

KANAMORI, H., Faulting of the Great Kanto earthquake of 1923 as revealed by seismological data, *Bull. Earthq. Res. Inst.*, **49** (1971), 13-18.

KANAMORI, H., and MIYAMURA, S., Seismometrical re-evaluation of the great Kanto earthquake of September 1, 1923, *Bull. Earthq. Res. Inst.*, **48** (1970), 115-125.

KANEKO, S., Right-lateral faulting in Miura peninsula, south of Tokyo, Japan, *Bull. Geol. Soc. Japan*, **75** (1969), 199-208.

KASAHARA, K., Physical conditions of earthquake faults II, *Bull. Earthq. Res. Inst.*, **37** (1959), 39-51.

KASAHARA, K., Geophysical monitoring system proposed for the earthquake prediction research project in the South-Kanto province, *Report of the Earthquake Prediction Observation Center, Earthq. Res. Inst. Tokyo Univ.*, **1** (1970), 25-31 (in Japanese).

KAWASUMI, H., Measures of earthquake danger and expectancy of maximum intensity throughout Japan as inferred from the seismic activity in historical time, *Bull. Earthq. Res. Inst.*, **29** (1951), 469-482.

KIMURA, M., KAGAMI, H., HONZA, E. and NASU, N., Stratigraphy and structure of continential shelves, slopes and canions in Sagami bays, *Bull. Ocean Res. Tokyo Univ.*, (1971), (in preparation).

MARUYAMA, T., Statical elastic dislocations in an infinite and semi-infinite medium, *Bull. Earthq. Res. Inst.*, **42** (1964), 289-368.

MATSUDA, T., Geologic provinces and active faults in the southern Kanto district, *Report of the Earthquake Prediction Observation Center, Earthq. Res. Inst. Tokyo Univ.*, **1** (1970), 9-16 (in Japanese).

MIYABE, N., On the vertical earth movement in Kwanto districts, *Bull. Earthq. Res. Inst.*, **9** (1934), 1-21.

MOGI, A., The submarine topography in the eastern and western parts of Sagami bay, *Hydrographic Bull. Special Number (Maritime Safety Board)*, **17** (1955), 117-127 (in Japanese).

MUTO, K., A study of displacements of triangulation points, *Bull. Earthq. Res. Inst.*, **10** (1932), 394-391.

SAVAGE, J.C. and HASTIE, L.M., Surface deformation associated with dip-slip faulting, *J. Geophys. Res.*, **71** (1966), 4897-4904.

SAVAGE, J.C. and HASTIE, L.M., A dislocation model for the Fairview peak Nevada earthquake, *Bull. Seism. Soc. Am.*, **59** (1969), 1937-1948.

PLAFKER, G. and SAVAGE, J.C., Mechanism of the Chilean earthquakes of May 21 and 22, 1960, *Bull. Geol. Soc. Am.*, **81** (1970), 1001-1030.

WALSH, J.B., Dip angle of faults as calculated from surface deformation, *J. Geophys. Res.*, **74** (1969) 2070-2980.

3. 地殻変動から求めた 1923 年関東大地震の震源パラメーター

地震研究所　安藤雅孝

1923 年の関東大地震の震源パラメーターを地殻変動を使つて推定した.

使つた資料は，陸地測量部の結果を modify して得た武藤の水平変動と宮部の垂直変動の結果である.

断層面は，半無限弾性体に長方形に切れ込まれた切れ目とし，その面上での変位は一様なものとした．このようにして表面の変位を丸山の式を使つて求め，地殻変動の data を最も良く説明する pattern を与える震源パラメーターを探した.

得られた値は，

断層面	長さ	130 km
	幅	65 km
	dip	45°
	dip direction	N45°E
断層面上の運動		
	thrust component	3 m
	right-lateral component	6 m

なお断層面と地表との交線は，地質及び地形的な証拠から，国府津 N45°W 付近をの方向に走る線と仮定した.

地殻変動から求めた震源パラメーターは，地震波から得られたものと良く一致している．ただし slip の量は前者の方が後者より 3 倍程大きい.

この地震は，日本海溝と伊豆マリアナ海溝との会合点から相模湾に伸びる相模トラフによつて境いされる 2 つの crust のブロックの差動的な運動によつて起こされたものと考えられる.